Electrical properties, texture, and microstructure of vicinal YBa$_2$Cu$_3$O$_{7-\delta}$ thin films

J. D. Pedarnig,[a] R. Rössler, M. P. Delamare, W. Lang,[b] and D. Bäuerle
Angewandte Physik, Johannes-Kepler-Universität Linz, A-4040 Linz, Austria

A. Köhler and H. W. Zandbergen
National Center for HREM, Delft University of Technology, Rotterdamseweg 137, NL-2628 AL Delft, The Netherlands

Vicinal YBa$_2$Cu$_3$O$_{7-\delta}$ (YBCO) thin films of thickness $h = 20-480$ nm are grown by pulsed-laser deposition on 10° miscut (001) SrTiO$_3$ substrates. The anisotropic resistivities, c-axis texture, and critical temperature drastically depend on the thickness of vicinal films. High-resolution electron microscopy reveals a defect microstructure with strong bending of the YBCO lattice near the SrTiO$_3$ interface and improved film microstructure at larger distances to the substrate. The required layer thickness for microstructure relaxation and increase of electrical conductivity are significantly larger than the critical thickness of c-axis oriented YBCO films. © *2002 American Institute of Physics.* [DOI: 10.1063/1.1508418]

High-temperature superconductors (HTS) have a quasi two-dimensional structure and reveal strongly anisotropic physical properties. For HTS thin films on single crystal substrates the c-axis orientation is energetically favored and only the ab-plane transport properties can be measured. However, on miscut substrates a coherently tilted, vicinal structure of the films can develop and the transport properties within the ab plane and along the c axis can be derived on the very same sample. Vicinal films are especially important for the characterization of materials which are not available as phase pure single crystals[1] and for the investigation of phenomena occurring in thin layers of a material.[2,3] Vicinal Bi$_2$Sr$_2$CaCu$_2$O$_{8+\delta}$ (Bi-2212) thin films show anisotropic resistivities independent of film thickness h in the range $h = 20-300$ nm.[4] These results are in striking contrast to the resistivity behavior of vicinal YBa$_2$Cu$_3$O$_{7-\delta}$ films.

In this letter we report on vicinal YBa$_2$Cu$_3$O$_{7-\delta}$ (YBCO) thin films ($h = 20-480$ nm) which reveal an extremely strong increase of resistivities and a reduced c-axis texture for thicknesses less than 100 nm. YBCO films are grown by pulsed-laser deposition (PLD) on miscut (001) SrTiO$_3$ substrates. UV-excimer laser pulses ($\lambda = 248$ nm, $\tau_L \approx 20$ ns, repetition rate 10 Hz, fluence 3.25 J/cm^2) are employed for target ablation.[6] The vicinal angle is $\theta_s = 10°$ and the substrates polished after cutting have a rms surface roughness of less than 0.2 nm (TBL Kelpin).

The thickness of vicinal YBCO films linearly increases with the number of laser pulses employed for target ablation. The deposition rate is 0.34 ± 0.01 Å/pulse. The vicinal films have a step-like surface morphology due to step-flow growth as observed by atomic force microscopy.[7,8] The film terraces are smooth and inclined by an angle $\theta = 9.5° \pm 1.7°$ with respect to the macroscopic film surface in good agreement to the nominal substrate miscut angle. Due to the bunching of

small steps with unit-cell height[9] relatively large terraces of width 107 ± 27 nm and steps of height 18 ± 6 nm are formed for films of 75 nm thickness. The anisotropic resistivities of vicinal YBCO films $\rho_P(T)$ and $\rho_O(T)$ were obtained from far-point measurements on current tracks oriented parallel and orthogonal to the vicinal steps, respectively. The in-plane $\rho_{ab}(T)$ and out-of-plane $\rho_c(T)$ resistivities were calculated from a rotation of the resistivity tensor by an angle θ_S and are $\rho_{ab} = \rho_P$ and $\rho_c = (\rho_O - \rho_{ab} \times \cos^2 \theta_S)/\sin^2 \theta_S$. Figure 1 summarizes the resistivity measurements on films with thick-
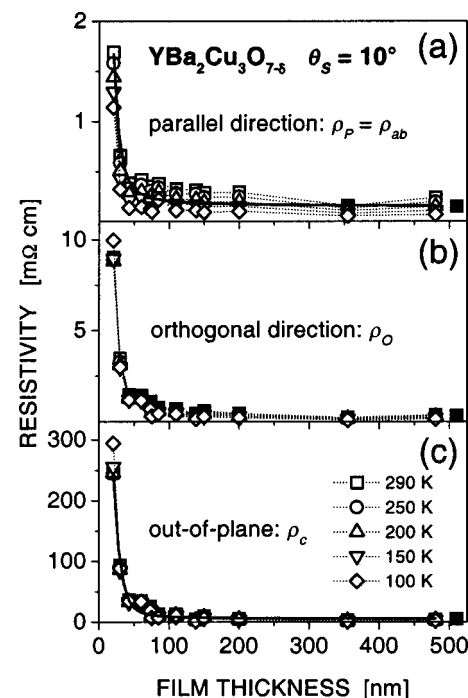

FIG. 1. Thickness and temperature dependence of anisotropic resistivities of vicinal YBCO thin films. Resistivities parallel (a) and orthogonal (b) to the vicinal steps and along the c-axis direction (c) strongly increase for thinner films. The squared solid symbols are YBCO single crystal resistivity data. Solid curves are a fit to the data.

[a]Electronic mail: johannes.pedarnig@jku.at
[b]On leave from: Institut für Materialphysik, Universität Wien, A-1090 Wien, Austria.

nesses $h=20-480$ nm. The resistivities very strongly depend on film thickness and progressively increase as the thickness decreases ($h<100$ nm). For films with thickness larger than 150 nm the resistivity values agree very well with YBCO single crystal data ($\rho_{ab}\approx0.15$ mΩ cm, $\rho_c \approx5.3$ mΩ cm, and $\rho_O\approx0.31$ mΩ cm at 290 K).[10] The films reveal a metallic conductivity behavior in the normal state (100 K$\leq T\leq290$ K). Only for the thinnest films ($h \leq30$ nm) the resistivities ρ_O and ρ_c show a slight increase for temperatures close to the superconducting phase transition. The onset temperature of the phase transition is 92 ±1 K for all films. The critical temperature depends on film thickness and is $T_{c0}\geq90$ K ($h\geq60$ nm), $T_{c0}=84$ K ($h =30$ nm), and $T_{c0}\approx50$ K ($h=20$ nm). For films of thicknesses of 60–320 nm, the resistivities $\rho_P(T)$ and $\rho_O(T)$ agree with other reports.[5] However, the drastic increase of resistivities for $h<60$ nm was not reported. The results in Ref. 5 were obtained from vicinal YBCO films grown on high-temperature annealed SrTiO$_3$ substrates which show a more regular surface structure than the substrates used in this study.[11] In order to check the influence of growth kinetics on layer properties, vicinal films ($h=75$ nm) were grown at low laser pulse repetition rate (1 Hz) for comparison. However, resistivity measurements and texture analysis showed the same results independent of repetition rate. Oxygen postannealing (800 mbar, $T\leq575$ °C) of patterned films increases resistivities and decreases $T_{c0}<50$ K of the thinnest films ($h\leq30$ nm) but does not change the properties of thicker films. These results indicate strongly modified materials properties as compared to YBCO for very thin layers.

The crystallinity of vicinal YBCO films was investigated by x-ray diffraction (XRD) using a three-circle goniometer with two-dimensional detection system (Cu $K\alpha$). All XRD peaks were due to (00ℓ) reflections from the Y-123 phase and secondary phases were not detected. The in-plane and out-of-plane texture of the vicinal films were measured by so-called φ scans and ω scans, respectively. The ω scans were performed for different orientation of the vicinal films with respect to the plane of x-ray incidence. For the "parallel" configuration, the film is aligned with the vicinal steps oriented parallel to the plane of incidence. Rocking curve peak intensities of the (005) YBCO and (002) SrTiO$_3$ reflections are measured at $\omega=\theta-\theta_B=0°$, where θ is the angle of incidence and ω denotes the relative scan angle. The Bragg angles of YBCO and SrTiO$_3$ are $\theta_B=19.30°$ and $\theta_B =23.26°$, respectively. In the orthogonal direction, the substrate miscut and vicinal film structure cause a shift of peak positions and the maximum intensities are measured at $\omega\cong \pm\theta_S$. In Fig. 2 the rocking curve half widths $\Delta\omega_{FWHM}$ are shown for the measurements parallel and orthogonal to the vicinal steps. The widths strongly increase for film thicknesses $h\leq100$ nm. The deviation from perfect c-axis alignment is stronger for the orthogonal direction demonstrating anisotropic crystallinity of films grown on miscut substrates. The dependence of widths on film thickness follows an exponential decay law, $\Delta\omega_{FWHM}=a+b\exp(-h/d)$ (solid curves in Fig. 2). The obtained relaxation lengths d are 45 ±6 nm and 49±4 nm for the parallel and orthogonal directions, respectively. The vicinal films are strongly in-plane textured with the a and b axes aligned parallel to the sub-
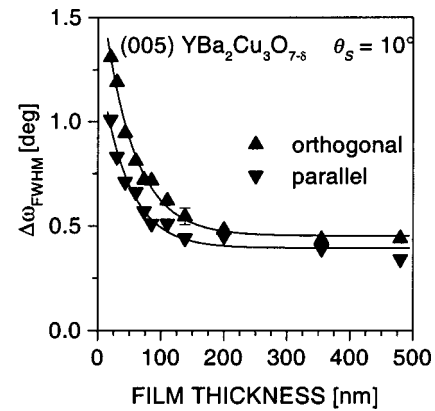

FIG. 2. Thickness dependence of the (005) YBCO rocking curve half width of vicinal films. The widths strongly increase for thinner films. The c-axis alignment is stronger for measurements parallel to the vicinal steps than for the orthogonal direction. Solid curves are a fit to the data.

strate lattice axes. The width of the (104) YBCO peak is $\Delta\varphi_{FWHM}\approx0.9°$ ($h=60$ nm) and $\Delta\varphi_{FWHM}\approx0.6°$ ($h =200$ nm).

The microstructure of vicinal YBCO thin films was investigated by high-resolution electron microscopy (HREM). Ion-beam milling of the samples was performed at low energy and small angle of incidence to avoid sample damage. In Fig. 3, HREM cross-section images are taken perpendicular [Figs. 3(a) and 3(c)] and parallel [Fig. 3(b)] to the direction of vicinal steps. Figures 3(a) and 3(b) are taken at the substrate interface. White lines indicate the orientation of ab planes in the YBCO film. In the direction perpendicular to the vicinal steps the film lattice is inclined by $\sim10°$ against the interface [dashed line, Fig. 3(a)]. In the direction parallel to the steps the lattice is oriented parallel to the interface [Fig. 3(b)]. HREM images reveal different kinds of imperfections: lattice bending and increased c spacings (indicated by white arrows in Fig. 3) and nanoscale inclusions. Also a doubling of the a or b axis can be observed locally. The increased c spacings, the doubling of the a axis, and part of the lattice bending, which occur in particular close to the interface with the substrate, are probably due to an intercalation of Cu–O planes or formation of CO$_x$.[12] Although the deteriorated film structure at the interface can be due to HREM sample preparation, such a strong deterioration does not occur in the rest of the film, indicating that at least it must be initiated by imperfections that were already present in the as prepared films. These local structural imperfections result in changes in the c direction, as was confirmed by x-ray diffraction. At larger distances from the interface no intercalation related lattice distortions are observed [Fig. 3(c), taken at a distance of ~70 nm to the interface]. Other defects in the vicinal films include antiphase boundaries and crystalline inclusions of rectangular shape (not shown in Fig. 3). Such inclusions have sizes around 5×20 nm^2 and are inclined against the substrate surface with their long and short axes oriented parallel and perpendicular to the basal plane of the surrounding YBCO matrix, respectively. The inclusions show fringes oriented parallel to the c axis of YBCO with a spacing of ~7.5 Å. From this it is concluded that the inclusions are probably Y$_2$O$_3$[13] with an orientation [110] Y$_2$O$_3$$\|$[100] Y-123. The Y$_2O_3$ phase is not in equilib-

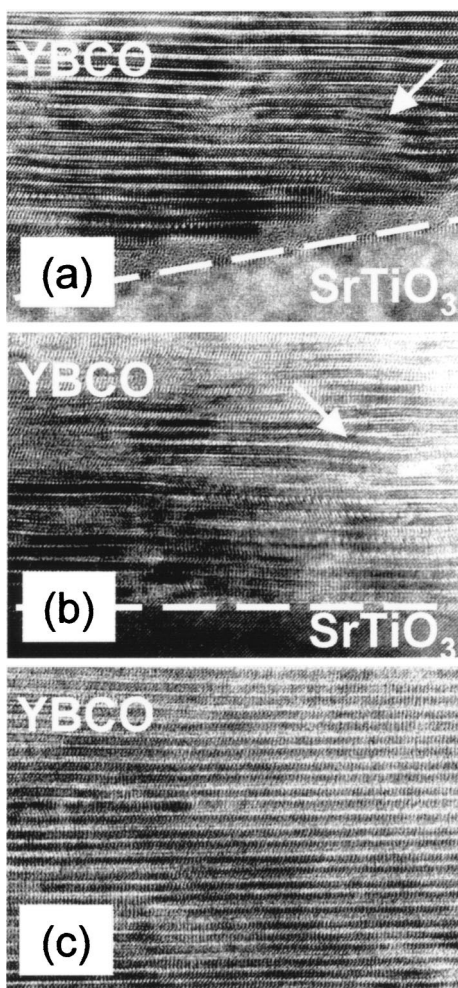Appl. Phys. Lett., Vol. 81, No. 14, 30 September 2002

Pedarnig *et al.* 2589

FIG. 3. HREM cross-section images of vicinal YBCO thin films taken at the substrate interface (a) and (b) and at a distance of ~70 nm to the interface (c). Perpendicular to the vicinal steps (a) the film lattice is inclined by ~10° against the substrate surface (indicated by dashed line). In the parallel direction the film is oriented parallel to the substrate surface (b). Lattice bending and increased c spacings are indicated by white arrows. Microstructure defects are not observed at larger distances from the interface (c).

rium with Y-123 at the deposition temperature of PLD films (typically 750 °C) but its formation is explained by "epitaxial phase stabilization." [14]

The resistivity, XRD and HREM results demonstrate that imperfections of the vicinal film microstructure near the interface vanish as the film thickness increases. The formation of a defect microstructure is probably due to the substrate surface and the film nucleation behavior. The off-axis cut (001) $SrTiO_3$ crystals have disordered surfaces with terraces of different heights and widths and kinked step edges which introduce defects in the YBCO epilayer. The nucleation of YBCO films on vicinal $SrTiO_3$ surfaces occurs via the formation of semiconducting perovskite $(Y,Ba)CuO_{3-x}$. [15] With increasing film thickness the development of continuous and highly conducting CuO_2 planes requires the formation of the Y-123 phase and the annihilation of defects. The observed thickness dependence of resistivities may be ascribed to a conductivity of films $\sigma(z)$ that changes with distance z to the interface. Charge carrier scattering at structural defects and modifications of the local charge carrier density possibly reduce the conductivity at the interface. At larger distances from the interface the conductivity may approach the single crystal values (σ_{YBCO}). The solid lines in Figs. 1(a) and 1(c) are fits employing $\sigma(z) = \sigma_{YBCO}/[1 + u \exp(-gz)]$ and averaging over film thickness h ($T = 290$ K). A linear or exponential variation of conductivity does not deliver satisfactory agreement to the anisotropic resistivities. The obtained relaxation lengths of the in-plane and out-of-plane conductivities, 31 ± 5 nm and 45 ± 2 nm, are comparable to the relaxation lengths of c-axis texture and the critical thickness $h_c = 30$ nm for films with $T_{c0} > 77$ K. The anisotropy of conductivity relaxation and crystallinity relaxation is probably due to the substrate miscut and the modified growth mode for vicinal films. For c-axis oriented YBCO films on (001) $SrTiO_3$ the critical thickness $h_c \approx 13$ nm is related to interfacial epitaxial strain [16] with a relaxation distance of 13.5 nm. [17] The Stranski–Krastanov transition from layer-by-layer to island growth occurs in the thickness range 9–19 nm. [18] The strikingly different behavior of vicinal Bi-2212 films ($h = 20-300$ nm) is possibly due to different materials properties. The relatively weak Van der Waals forces and the easy shearing of Bi-2212 half cells may contribute to shorter relaxation lengths of epitaxial strain and structural defects at the interface.

[1] S. H. Yun, R. Rössler, J. D. Pedarnig, D. Bäuerle, and X. Obradors, Appl. Phys. Lett. **77**, 1369 (2000).

[2] P. Berghuis, E. Di Bartolomeo, G. A. Wagner, and J. E. Evetts, Phys. Rev. Lett. **79**, 2332 (1997).

[3] W. Markowitsch, C. Stockinger, W. Lang, K. Bierleutgeb, J. D. Pedarnig, and D. Bäuerle, Appl. Phys. Lett. **71**, 1246 (1997).

[4] R. Rössler, J. D. Pedarnig, D. Bäuerle, E. J. Connolly, and H. W. Zandbergen, Appl. Phys. A: Mater Sci. Process **A71**, 245 (2000).

[5] T. Haage, J. Zegenhagen, J. Q. Li, H.-U. Habermeier, M. Cardona, Ch. Jooss, R. Warthmann, A. Forkl, and H. Kronmüller, Phys. Rev. B **56**, 8404 (1997).

[6] D. Bäuerle, *Laser Processing and Chemistry*, 3rd ed. (Springer, Berlin, 2000).

[7] D. H. Lowndes, X.-Y. Zheng, S. Zhu, J. D. Budai, and R. J. Warmack, Appl. Phys. Lett. **61**, 852 (1992).

[8] W. A. M. Aarnink, E. M. C. M. Reuvekamp, M. A. J. Verhoeven, M. V. Pedyash, G. J. Gerritsma, A. van Silfhout, H. Rogalla, and T. W. Ryan, Appl. Phys. Lett. **61**, 607 (1992).

[9] L. Méchin, P. Berghuis, and J. E. Evetts, Physica C **302**, 102 (1998).

[10] K. Takenaka, K. Mizuhashi, H. Takagi, and S. Uchida, Phys. Rev. B **50**, 6534 (1994).

[11] J. Zegenhagen, T. Haage, and Q. D. Jiang, Appl. Phys. A: Mater Sci. Process **A67**, 711 (1998).

[12] H. W. Zandbergen, R. J. Cava, J. J. Krajewski, and W. F. Peck, Jr., Physica C **179**, 227 (1991).

[13] K. Verbist, A. L. Vasiliev, and G. Van Tendeloo, Appl. Phys. Lett. **66**, 1424 (1995).

[14] S. V. Samoylenkov, O. Yu. Gorbenko, I. E. Graboy, A. R. Kaul, H. W. Zandbergen, and E. Connolly, Chem. Mater. **11**, 2417 (1999).

[15] T. Haage, J. Zegenhagen, H.-U. Habermeier, and M. Cardona, Phys. Rev. Lett. **80**, 4225 (1998).

[16] L. X. Cao, J. Zegenhagen, E. Sozontov, and M. Cardona, Physica C **337**, 24 (2000).

[17] W. J. Lin, P. D. Hatton, F. Baudenbacher, and J. Santiso, Appl. Phys. Lett. **72**, 2966 (1998).

[18] X. Y. Zheng, D. H. Lowndes, S. Zhu, J. D. Budai, and R. J. Warmack, Phys. Rev. B **45**, 7584 (1992).